

Galaxy counterparts of metal-rich damped $\text{Ly}\alpha$ absorbers – II. A solar-metallicity and dusty DLA at $z_{\text{abs}} = 2.58^*$

J. P. U. Fynbo,^{1†} C. Ledoux,² P. Noterdaeme,³ L. Christensen,⁴ P. Møller,⁵ A. K. Durgapal,⁶ P. Goldoni,^{7,8} L. Kaper,⁹ J.-K. Krogager,¹ P. Laursen,¹⁰ J. R. Maund,^{1,11} B. Milvang-Jensen,¹ K. Okoshi,¹² P. K. Rasmussen,¹³ T. J. Thorsen,¹ S. Toft¹ and T. Zafar¹

¹Dark Cosmology Centre, Niels Bohr Institute, Copenhagen University, Juliane Maries Vej 30, 2100 Copenhagen O, Denmark

²European Southern Observatory, Alonso de Córdova 3107, Vitacura, Casilla 19001, Santiago 19, Chile

³Departamento de Astronomía, Universidad de Chile, Casilla 36-D, Santiago, Chile

⁴Excellence Cluster Universe, Technische Universität München, Boltzmanstrasse 2, 85748 Garching bei München, Germany

⁵European Southern Observatory, Karl-Schwarzschildstrasse 2, 85748 Garching bei München, Germany

⁶Department of Physics, DSB Campus Kumaun University, Nainital, Uttarakhand, India

⁷Laboratoire Astroparticule et Cosmologie, 10 rue A. Domon et L. Duquet, 75205 Paris Cedex 13, France

⁸Service d'Astrophysique, DSM/IRFU/Sap, CEA-Saclay, 91191 Gif-sur-Yvette, France

⁹Astronomical Institute 'Anton Pannekoek', University of Amsterdam, Kruislaan 403, 1098 SJ Amsterdam, the Netherlands

¹⁰Oskar Klein Centre, Department of Astronomy, Stockholm University, 10691 Stockholm, Sweden

¹¹Department of Astronomy and Astrophysics, University of California, Santa Cruz, CA 95064, USA

¹²Tokyo University of Science, Oshamanbe, Hokkaido, 049-3514 Tokyo, Japan

¹³Niels Bohr Institute, Copenhagen University, Juliane Maries Vej 30, 2100 Copenhagen O, Denmark

11 January 2011

ABSTRACT

This is the second paper in a series reporting on results from a survey conducted with the ESO VLT/X-shooter spectrograph. We target high metallicity damped Lyman- α absorbers (DLAs) with the aim of investigating the relation between galaxies detected in emission and those detected in absorption. Here, we report on the discovery of the galaxy counterpart of the $z_{\text{abs}} = 2.58$ DLA on the line-of-sight to the $z = 3.07$ quasar SDSS J091826.16+163609.0 (hereafter Q 0918+1636). The galaxy counterpart of the DLA is detected in the [OIII] $\lambda 5007$ and [OI] $\lambda\lambda 3726, 3729$ emission lines redshifted into the NIR at an impact parameter of 2.0 arcsec (16 kpc at $z = 2.58$). $\text{Ly}\alpha$ emission is not detected down to a 3σ detection limit of $5 \times 10^{-18} \text{ erg s}^{-1} \text{ cm}^{-2}$, which, compared to the strength of the oxygen lines, implies that $\text{Ly}\alpha$ emission from this galaxy is suppressed by more than an order of magnitude. The DLA has one of the highest metallicities measured so far at comparable redshifts. We find evidence for substantial depletion of refractory elements onto dust grains. Fitting the main metal line component of the DLA, which is located at $z_{\text{abs}} = 2.5832$, we measure metal abundances from ZnII, SiII, SiIII, CrII, MnII, FeII and NiII of -0.12 ± 0.05 , -0.26 ± 0.05 , -0.46 ± 0.05 , -0.88 ± 0.05 , -0.92 ± 0.05 , -1.03 ± 0.05 and -0.78 ± 0.05 , respectively. In addition, we detect absorption in the Lyman and Werner bands of molecular hydrogen (H_2), which represents the first detection of H_2 molecules with X-shooter. The background quasar Q 0918+1636 is amongst the reddest QSOs at redshifts $3.02 < z < 3.12$ from the SDSS catalogue. Its UV to NIR spectrum is well fitted by a composite QSO spectrum reddened by SMC/LMC-like extinction curves at $z_{\text{abs}} = 2.58$ with a significant amount of extinction given by $A_V \approx 0.2 \text{ mag}$. This supports previous claims that there may be more metal-rich DLAs missing from current samples due to dust reddening of the background QSOs. The fact that there is evidence for dust both in the central emitting regions of the galaxy (as evidenced by the lack of $\text{Ly}\alpha$ emission) and at an impact parameter of 16 kpc (as probed by the DLA) suggests that dust is widespread in this system.

Key words: galaxies: formation – galaxies: high-redshift – galaxies: ISM – quasars: absorption lines – quasars: individual: SDSS J091826.16+163609.0 – cosmology: observations

1 INTRODUCTION

The comparison between absorption-line selected and emission-selected galaxies at redshifts $z > 2$ has a long history (e.g., Smith et al. 1989; Møller & Warren 1993; Wolfe et al. 2005, and references therein). However, progress in this field has been slow and, for many years, there has been little overlap between observational samples (e.g., Fynbo et al. 1999; Møller et al. 2002; Colbert & Malkan 2002; Kulkarni et al. 2006). Recently, some progress has been made though in order to build the bridge between the two populations. Emission-selected galaxies have been studied to much deeper rest frame flux limits than a decade before (e.g., Sawicki & Thompson 2006; Gronwall et al. 2007; Rauch et al. 2008; Ouchi et al. 2008; Grove et al. 2009; Reddy & Steidel 2009; Cassata et al. 2011). Fynbo et al. (2010, hereafter F10) also presented the first results from a small survey to search for the galaxy counterparts of metal-rich damped Ly α absorbers (DLAs; see Wolfe et al. 2005, for a review). In F10, the detection of the galaxy counterpart of a high-metallicity DLA at $z_{\text{abs}} = 2.354$ toward Q2222–0946 was presented. F10 described the strategy and sample selection of the survey in details. Here, we reiterate that the candidates were selected amongst SDSS QSOs based on the strengths of SiII and FeII absorption lines (i.e., not directly from Ly α).

In this paper, we present new results based on observations of the second target of the survey, the $z = 3.07$ quasar SDSS J091826.16+163609.0 (hereafter Q0918+1636). Q0918+1636 was selected as its spectrum features a metal-rich absorber at $z = 2.412$ having rest frame equivalent widths (EWs) of the targeted SiII λ 1526 and FeII $\lambda\lambda$ 2344, 2374, 2382 lines of 2.1 Å, 2.1 Å, 1.4 Å and 2.6 Å, respectively. The properties of this absorber will be the subject of another paper describing a sample of objects. For now, we note that this absorber, which is also a DLA, has a high metallicity with [Si/H] = −0.6. Here, we describe the serendipitous discovery and properties of a second DLA, at $z_{\text{abs}} = 2.5832$, along the line-of-sight to Q0918+1636. This system happens to also fulfill our sample selection criteria, with rest frame EWs of 2.4 Å, 2.4 Å, 1.6 Å and 3.0 Å for SiII λ 1526 and FeII $\lambda\lambda$ 2344, 2374, 2382, respectively. The FeII lines from this system are redshifted outside of the wavelength interval suited for automatic searches of absorption lines in SDSS spectra and hence were not identified. Interestingly also, neither of the two DLAs in this QSO spectrum have been identified in automatic DLA (i.e., Ly α -based) searches in SDSS (Prochaska et al. 2005; Noterdaeme et al. 2009b). This is due to a recently identified bias against the detection of damped Lyman-alpha absorption lines at the blue end of the spectra (see Noterdaeme et al. 2009b). Indeed, the signal-to-noise ratio is decreased significantly by the presence of any strong and/or several closeby DLA lines.

Throughout this paper, we assume a flat cosmology with

$\Omega_{\Lambda} = 0.70$, $\Omega_m = 0.30$ and a Hubble constant of $H_0 = 70 \text{ km s}^{-1} \text{ Mpc}^{-1}$.

2 OBSERVATIONS AND DATA REDUCTION

Q0918+1636 was observed on February 16 2010 with X-shooter at the VLT. The QSO was observed at three position angles (PAs), namely 60°, −60° and 0° (all East of North). The purpose of using three slit positions is to cover a larger field of view around the QSO as shown in fig. 1 of F10. The integration time at each PA was 3600 s, and a 1.3''-wide slit in the UVB arm and 1.2''-wide slits in the VIS and NIR arms were used.

The expected resolving power with the above setup is 4000, 6700 and 4300 in the UVB, VIS and NIR arms, respectively. This is confirmed by the width of sky emission lines in the spectra. However, the seeing during the observations was significantly smaller than the widths of the slits (i.e., 0.67 arcsec in all three exposures as measured from the width of the QSO trace around 7500 Å) and hence the true spectral resolution is higher than that measured from sky emission lines. In the VIS arm, we measure the resolution directly from the width of telluric absorption lines. We then assume that the ratio between expected and true resolutions is the same in all three spectroscopic arms, and the degradation of seeing as a function of decreasing wavelength is calculated as the ratio of the wavelengths to the power of 0.2. In this way, we infer resolving power values of 6400, 11900 and 8800 in the UVB, VIS and NIR arm, respectively.

We processed the spectra using the X-shooter data reduction pipeline (see Goldoni et al. 2006, see also F10). First, raw frames were corrected for the bias level (UVB and VIS) or dark current (NIR). Then, after background subtraction, cosmic ray hits were detected and removed using the method developed by van Dokkum (2001) while sky emission lines were subtracted using the method described in Kelson (2003). After division by a master flat-field, the spectral orders were extracted and rectified in wavelength space using a wavelength solution previously obtained from calibration frames. The orders were then merged and in their overlapping parts the merging was weighted by the corresponding errors which were propagated in the process. From the resulting merged 2D spectrum, a one-dimensional spectrum of the QSO was extracted. This 1D spectrum together with its error file and bad-pixel map are the final products of the reduction. Intermediate products such as the sky spectrum and individual echelle orders (with errors and bad-pixel maps) were also produced. The spectra were flux-calibrated using a spectrophotometric standard star observed during the same night. The flux calibration was checked against the flux-calibrated SDSS QSO spectrum and found to be consistent with it.

3 RESULTS

3.1 Emission properties of the DLA-galaxy counterpart

We do not detect Ly α emission at any of the three position angles (see Fig. 1). We calculate a conservative 3σ detection limit from a $1000 \text{ km s}^{-1} \times 2.0 \text{ arcsec}$ square aperture inside the trough of

* Based on observations carried out under prog. ID 084.A-0303 with the X-shooter spectrograph installed at the Cassegrain focus of the Very Large Telescope (VLT), Unit 2 – Kueyen, operated by the European Southern Observatory (ESO) on Cerro Paranal, Chile.

† E-mail: jfynbo@dark-cosmology.dk

the $z = 2.58$ damped $\text{Ly}\alpha$ absorption line. The velocity width of 1000 km s^{-1} is based on the $\text{Ly}\alpha$ line from the galaxy counterpart of the DLA towards Q 2222–0946 (F10, see also theoretical profiles in Laursen et al. (2010)), whereas the spatial width of 2 arcsec is based on the fact that $\text{Ly}\alpha$ emission can be quite extended (e.g., Møller & Warren 1998; Fynbo et al. 2003; Rauch et al. 2008). The resulting limit is $5 \times 10^{-18} \text{ erg s}^{-1} \text{ cm}^{-2}$. Assuming that all $\text{Ly}\alpha$ photons escape, case-B recombination and the relation between $\text{H}\alpha$ luminosity and star formation rate (SFR) from Kennicutt (1998), we would place an upper limit on the SFR of $0.3 \text{ M}_{\odot} \text{ yr}^{-1}$. Unfortunately, the expected position of the $\text{H}\alpha$ emission line is in a part of the NIR spectrum where the sky background is too high to allow for a useful detection limit to be derived. However, we do detect the $[\text{OIII}] \lambda 5007$ emission line in the $\text{PA} = 60^\circ$ spectrum at an impact parameter of 2.0 arcsec (see Fig. 1). The redshift of the $[\text{OIII}] \lambda 5007$ line is consistent with that of low-ionisation metal lines to within an uncertainty of about 50 km s^{-1} . This line is detected neither in the $\text{PA} = -60^\circ$ nor the $\text{PA} = 0^\circ$ spectra. We also detect both components of the $[\text{OII}] \lambda\lambda 3726, 3729$ doublet but with a lower signal-to-noise ratio and in a region somewhat affected by telluric absorption lines. The flux of the $[\text{OIII}] \lambda 5007$ line is $f = 1.7 \pm 0.2 \times 10^{-17} \text{ erg s}^{-1} \text{ cm}^{-2}$, which corresponds to a luminosity of $L = 9 \times 10^{41} \text{ erg s}^{-1}$. This is a lower limit due to the possibility of slit-loss. For the $[\text{OII}]$ doublet, we infer a total flux of about $2.5 \times 10^{-17} \text{ erg s}^{-1} \text{ cm}^{-2}$ after correcting for telluric absorption. Using the relation from Kennicutt (1998), we infer a SFR of about $20 \text{ M}_{\odot} \text{ yr}^{-1}$. Hence, $\text{Ly}\alpha$ emission from this system appears to be suppressed by more than an order of magnitude.

In order to exclude the possibility of the existence of a galaxy counterpart located at small impact parameter, we also performed spectral point spread function subtraction as in F10. No emission line is detected at an impact parameter smaller than 2 arcsec. Any line with a flux similar to or larger than the detected $[\text{OIII}]$ line would be detected in the data.

3.2 Absorption-line properties of the DLA

3.2.1 Metal lines

The total H I column density of the system is well constrained by the damped $\text{Ly}\alpha$ absorption line to be $\log N(\text{H I}) = 20.96 \pm 0.05$ (see Fig. 1), where the error is a conservative error on the uncertainty, which is dominated by the systematic error from the normalisation. In particular, the fact that the DLA line is located in the red wing of the OVI emission line of the QSO complicates the normalisation somewhat.

The absorption profiles of the strongest Fe II and Mg II lines span a velocity range of up to 600 km s^{-1} (see $\text{Fe II} \lambda 2382$ in the upper right panel of Fig. 2). However, most of the absorption as seen from unsaturated or weakly saturated lines from singly ionized species is concentrated within a single broad velocity component at $z_{\text{abs}} = 2.5832(2)$. In order to derive overall metallicities in the neutral gas phase, we focus on fitting this main component. For the fitting, we use the package FITLYMAN as available in MIDAS. From the weak $\text{Si III} \lambda 1808$ line, one can see that this main component is responsible for 85% of the total EW and hence most likely – at least – 85% of the total column density of low-ionisation species.

The results of Voigt-profile fitting are summarised in Table 1 and displayed in Fig. 2. The instrumental resolution FWHM is 47 and 25 km s^{-1} for the UVB- and VIS-arm spectra, respectively. With a broadening parameter $b = 52 \text{ km s}^{-1}$, the fitted metal-line profile is well-resolved. However, should it include in reality one or

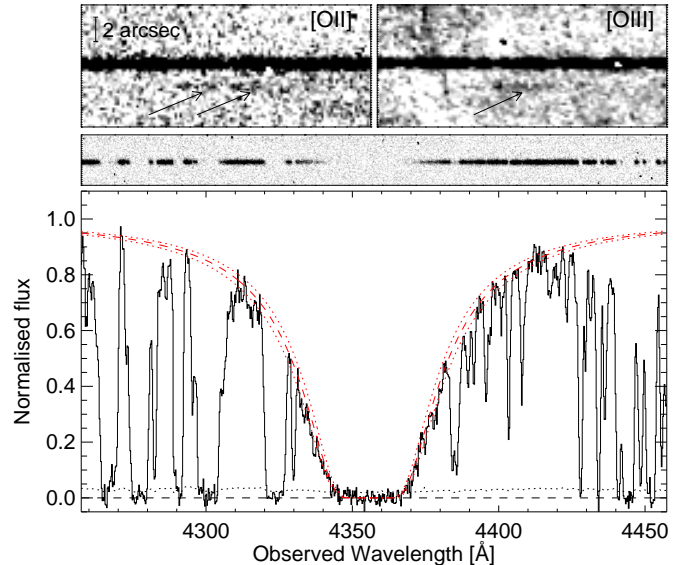


Figure 1. *Top panels:* The detected $[\text{OII}] \lambda\lambda 3726, 3729$ and $[\text{OIII}] \lambda 5007$ emission lines from the DLA-galaxy counterpart observed 2.0 arcsec away from the QSO continuum. The arrows point to the predicted centroids of the lines if these were at the same redshift as the low-ionisation absorption lines from the DLA. *Middle and bottom panels:* The region around $\text{Ly}\alpha$ from both the two- and one-dimensional spectra with $\text{PA} = 60^\circ$. As can be seen, the $\text{Ly}\alpha$ emission line is not detected. The red dashed and dotted lines show the Voigt profile fit to the damped $\text{Ly}\alpha$ line and associated 1σ uncertainties, respectively, corresponding to a neutral hydrogen column density of $\log N(\text{H I}) = 20.96 \pm 0.05$.

several narrow components, hidden saturation could be an issue and strictly speaking our measurements should be considered as lower limits. This means that the overall metallicity of this DLA could be even higher than solar. However, apart from Si II and to some extent also Si III , we are considering relatively weak absorption lines in the fitting process (see Fig. 2) so that the measured column densities for the corresponding species should depend weakly on individual b values if at all.

The usual complications of line blending in low-resolution spectra are avoided here as a single well-defined component is fit and therefore the presence of blending with unrelated absorption line features is easier to identify. Absorption from neutral carbon is detected ($\text{C I} \lambda\lambda 1560, 1656$) but due to blending with C I^* and C I^{**} lines neutral carbon is not considered in the analysis any further. Also, it is not possible to infer whether C II^* is present due to blending with the $\text{C II} \lambda 1334$ line which is highly saturated. Hence, we cannot determine the relative strengths of C II^* and C II and use them as diagnostics to infer the presence of local radiation fields (Wolfe et al. 2008). The errors given in Table 1 are the formal statistical errors from FITLYMAN. The systematic errors from, e.g., normalisation and not knowing the instrumental resolution precisely, are larger than this. An error of 0.05 dex would be a conservative estimate including all error sources.

The metallicity of the system is exceptionally high. From Zn II , which is little depleted onto dust grains (Meyer & Roth 1990), we infer a metallicity of -0.12 ± 0.05 . Note that the splitting between $\text{Zn II} \lambda 2026$ and $\text{Mg I} \lambda 2026$ is 50 km s^{-1} implying that Mg I cannot significantly contribute to the Zn II column density. Here, we adopt the solar photosphere abundances from Asplund et al. (2009). Given that we only fitted the main velocity component,

the overall metallicity of the DLA must be solar or higher than solar in case of hidden saturation. We also note that the $[\text{Mn}/\text{Fe}]$ ratio is larger than solar, which is only seen at or above solar metallicity (Ledoux et al. 2002). For elements which are sensitive to dust depletion (e.g., Meyer & Roth 1990; Pettini et al. 1997; Ledoux et al. 2002), we find $[\text{Fe}/\text{H}] = -1.03$, $[\text{Ni}/\text{H}] = -0.78$, $[\text{Mn}/\text{H}] = -0.92$, and $[\text{Cr}/\text{H}] = -0.88$ implying substantial dust depletion for these elements.

To compare the kinematics of the absorption-line profiles with that of other DLAs, we follow the procedure of Ledoux et al. (2006) and calculate the line-profile velocity width, ΔV , as $c[\lambda(95\%) - \lambda(5\%)]/\lambda_0$, where $\lambda(5\%)$ and $\lambda(95\%)$ are the wavelengths corresponding to, respectively, the 5 and 95 percentiles of the apparent optical depth distribution, and λ_0 is the first moment (the average) of this distribution (see fig. 1 of Ledoux et al. 2006). We again choose the SiII $\lambda 1808$ transition as it is a low-ionisation transition and the line is only mildly saturated. The apparent line optical depth and the derived velocity width are shown in Fig. 3. We infer a velocity width of 295 km s^{-1} in good agreement with the velocity-metallicity relation for DLAs (Ledoux et al. 2006).

3.2.2 Molecular absorption

Absorption lines from the Lyman and Werner bands of molecular hydrogen (H_2) are detected at $z = 2.5832$ in the X-shooter spectrum of Q 0918+1636 (see Fig. 4). The observed velocity extent of the H_2 profile is wider than the instrumental resolution FWHM (48 km s^{-1} at 3800 \AA) and much wider than the typical Doppler parameter of individual molecular lines as measured from high-resolution spectroscopy (usually $b \sim 3 \text{ km s}^{-1}$; Ledoux et al. 2003). This indicates that the actual H_2 profile comprises several blended components. Two absorption peaks separated by about 55 km s^{-1} can be distinguished in the H_2 profile, while they are not seen in the profile of metal lines that are fitted with a single component having $b = 52.1 \text{ km s}^{-1}$. This means that the metals are somehow continuously spread over $\text{FWHM} = b \times 2\sqrt{\ln 2} \sim 87 \text{ km s}^{-1}$, while the H_2 components are discrete and well-separated in velocity space. Indeed, this is a general behaviour as seen in other H_2 -bearing systems studied at high spectral resolution (e.g. Ledoux et al. 2002b).

In order to estimate the H_2 column density, we compared the data with synthetic profiles of H_2 absorption consisting of two components separated by 55 km s^{-1} built with the same spectral resolution and binning. We varied the column density in rotational levels from $J = 0$ to $J = 3$ for each component until we got a synthetic spectrum consistent with the data. We repeated this exercise for a wide range of Doppler parameters ($b = 1$ to 20 km s^{-1}) to get a realistic range on the total H_2 column density: $N(\text{H}_2) = 1.5 \times 10^{16} - 1.1 \times 10^{19} \text{ cm}^{-2}$. This corresponds to an overall molecular fraction $f = (2N(\text{H}_2))/(2N(\text{H}_2) + N(\text{H I})) = 3.3 \times 10^{-5} - 2.4 \times 10^{-2}$.

Details on the column densities in each rotational level and for the two components are given in Table 2. These measurements are only indicative and should be considered with caution because of the various uncertainties. Only high spectral resolution observations are suitable to properly resolve the H_2 line profile in individual components, measure accurately the column densities, and study the physical conditions in the gas (e.g., Srianand et al. 2005; Noterdaeme et al. 2007). Nevertheless, the presence of H_2 in this system is firmly established.

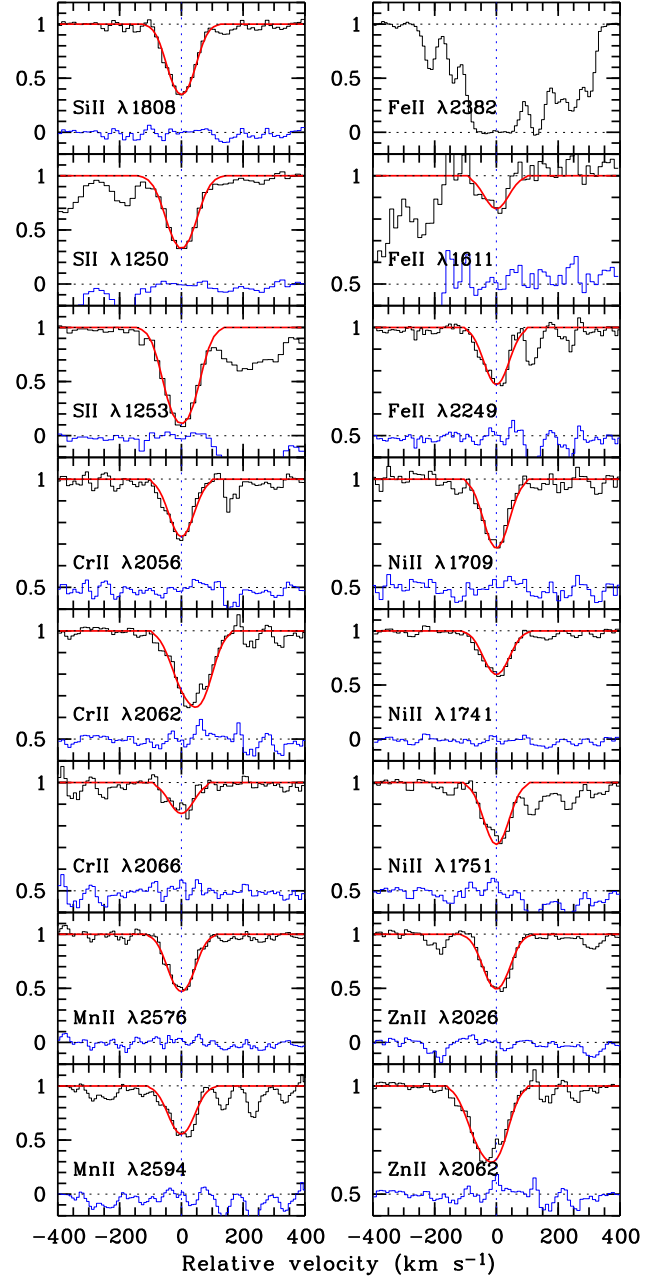


Figure 2. Results of Voigt-profile fits to low-ionisation lines from the $z_{\text{abs}} = 2.5832$ DLA toward Q 0918+1636. Most of the absorption is concentrated within one velocity component. In order to derive overall metallicities in the neutral gas phase, we focus on fitting this main component which is responsible for at least 85% of the total metal column density (see text). The Voigt-profile fits are shown with a red line and the residuals from the fits are shown with a blue line (for display purposes, a constant of 0.5 has been added to the residuals in some of the panels).

Table 1. Ionic column densities in the main metal-line component of the $z_{\text{abs}} = 2.5832$ DLA toward Q 0918+1636.

Ion	Transition lines used	$\log N \pm \sigma_{\log N}$	[M/H]	$b \pm \sigma_b$ (km s ⁻¹)
SiII	1808	16.01 ± 0.01	-0.46 ± 0.05	52.1 ± 0.5
SiII	1250,1253	15.82 ± 0.01	-0.26 ± 0.05	52.1 ± 0.5
CrII	2056,2062,2066	13.72 ± 0.01	-0.88 ± 0.05	52.1 ± 0.5
MnII	2576,2594	13.47 ± 0.01	-0.92 ± 0.05	52.1 ± 0.5
FeII	1611,2249	15.43 ± 0.01	-1.03 ± 0.05	52.1 ± 0.5
NiII	1709,1741,1751	14.40 ± 0.01	-0.78 ± 0.05	52.1 ± 0.5
ZnII	2026,2062	13.40 ± 0.01	-0.12 ± 0.05	52.1 ± 0.5

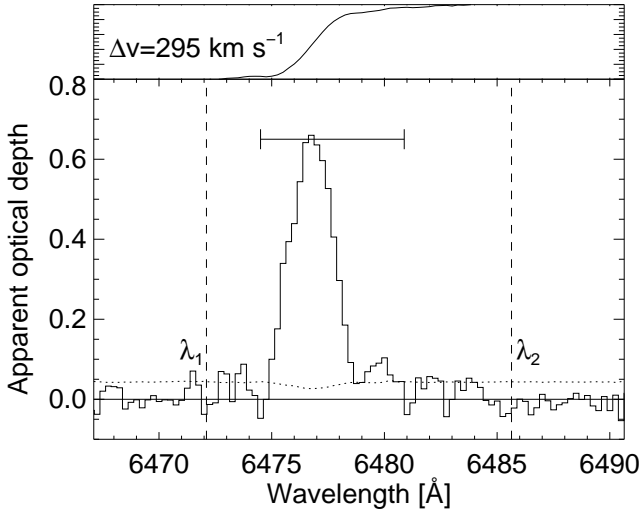


Figure 3. The profile of the SiII $\lambda 1808$ line. The profile consists of a main, broad component and a wing towards the red end of the profile. The velocity width of the line, measured following the method of Ledoux et al. (2006), is 295 km s^{-1} (marked with a horizontal segment). λ_1 and λ_2 are the start and end wavelengths used to integrate the profile.

Table 2. H₂ column densities. The velocities, Δv , of the two components are given in km s⁻¹ with respect to $z_{\text{abs}} = 2.5832$.

Rot. level component	$\log N \text{ (cm}^{-2}\text{)}$	
	$b=1 \text{ km s}^{-1}$	$b=20 \text{ km s}^{-1}$
$J = 0$	18.45	15.4
$\Delta v = -26$	18.2	15.1
$\Delta v = +28$	18.1	15.1
$J = 1$	18.75	15.85
$\Delta v = -26$	18.5	15.5
$\Delta v = +28$	18.4	15.6
$J = 2$	18.35	15.6
$\Delta v = -26$	18.2	15.3
$\Delta v = +28$	17.8	15.3
$J = 3$	17.7	15.0
$\Delta v = -26$	17.7	14.8
$\Delta v = +28$	16.4	14.6
Total	19.05	16.15

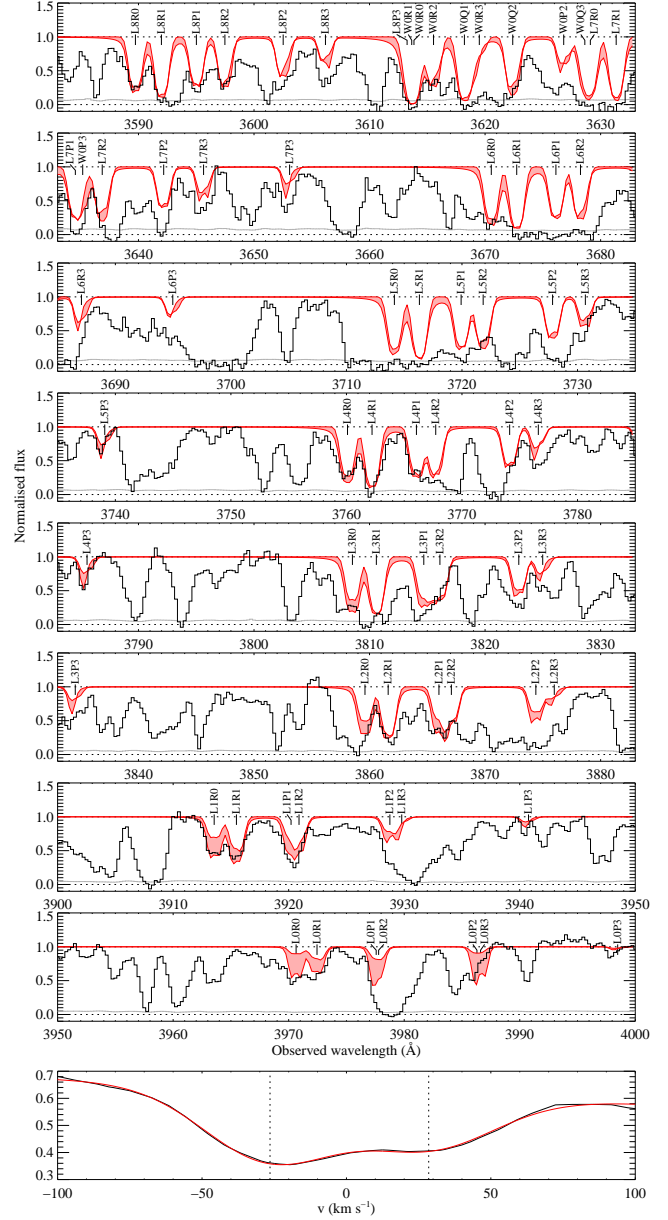


Figure 4. Portion of the X-shooter spectrum featuring H₂ absorption lines superimposed on the Ly α forest. The label over each absorption line indicates the band (L: Lyman, W: Werner), the vibrational level of the upper state, the branch (P, Q or R for $\Delta J = +1, 0, -1$, respectively) and the rotational level J of the lower state. The synthetic profiles corresponding to $b = 1$ and $b = 20 \text{ km s}^{-1}$ are overplotted as a shaded area. The bottom panel represents the stacking of unsaturated, unblended lines (LOR0, L1R0, L1R1, L4R0 and L8R0), revealing better the two peaks in the H₂ velocity profile.

4 DISCUSSION AND CONCLUSIONS

4.1 Nature of the DLA galaxy counterpart

The $z_{\text{abs}} = 2.5832$ DLA toward Q 0918+1636 is amongst the highest metallicity DLAs known to date (compared, e.g., to the sample of Kaplan et al. 2010). The fact that we detect the galaxy counterpart of this DLA is consistent with our suggestion that high metallicity DLAs should have bright galaxy counterparts (Møller et al. 2004; Fynbo et al. 2008, 2010). Indeed, stellar mass, metallicity and star formation rate in galaxies are in-

timately related (Mannucci et al. 2010). Galaxy mass-metallicity relations have been found to exist up to at least $z = 3.5$ (e.g., Tremonti et al. 2004; Savaglio et al. 2005; Erb et al. 2006; Kewley & Ellison 2008; Maiolino et al. 2008; Lamareille et al. 2009). The mass-metallicity relations at high redshift are steeper and offset towards higher stellar masses for a given metallicity compared to the relation observed in the local Universe (see, e.g., fig. 8 in Maiolino et al. 2008). Therefore, by selecting high-metallicity systems we should pick the most massive structures. In turn, because the star formation rate in galaxies is at any redshift correlated with total stellar mass (see fig. 1 in Dutton et al. 2010, and references therein), the most massive galaxies have expected star formation rates high enough ($\text{SFR} \gtrsim 10 \text{ M}_\odot \text{ yr}^{-1}$) to be detected with our observing method. It is encouraging that we have already found a second case after F10 in agreement with this reasoning.

The large impact parameter of 2.0 arcsec, corresponding to 16.0 kpc, is also consistent with the expectations from a simple model (see fig. 3 in Fynbo et al. 2008). The detection of H_2 absorption is consistent with the previously found trend that H_2 is predominantly found in high-metallicity (Petitjean et al. 2006) and dusty (Ledoux et al. 2003; Noterdaeme et al. 2008) systems. Unlike the system studied in F10, $\text{Ly}\alpha$ emission from the $z_{\text{abs}} = 2.5832$ DLA galaxy toward Q 0918+1636 is strongly suppressed. A plausible reason for this is dust obscuration given the high metallicity and the evidence for dust in the galaxy along the line-of-sight to the background QSO (Charlot & Fall 1991). Whereas we have no direct information on the amount of dust in the centre of the galaxy, presumably traced by the centroid of the line emission, it is likely to be higher than in the outer parts of the galaxy traced by the DLA.

4.2 $\text{Ly}\alpha$ escape fraction

Whereas the limit we infer for the $\text{Ly}\alpha$ luminosity is similar to the mean $\text{Ly}\alpha$ luminosity for DLA galaxies inferred by Rahmani et al. (2010) (see also Rauch & Haehnelt 2010) it is still very low compared to the strength of the [OIII] and [OII] emission lines from the galaxy.

The escape fraction f_{esc} of $\text{Ly}\alpha$ photons at high redshift is a highly coveted quantity as a plethora of interesting physical properties of galaxies can be revealed by studying this line. A number of authors have attempted to assess this matter, yielding quite different results; the standard procedure has been to compare the ratio of $\text{Ly}\alpha$ -inferred SFRs to those of other proxies with what is expected theoretically assuming case-B recombination, e.g., Le Delliou et al. (2005, 2006, a universal 2% from comparing observational data with modelled galaxies), Dayal et al. (2009, 30% from comparing simulated galaxies with observed luminosity functions), and Gawiser et al. (2006, 80% from comparing $\text{Ly}\alpha$ -inferred SFRs to spectral energy distribution (SED) modelling of observed $\text{Ly}\alpha$ emitters). Laursen et al. (2009b), using the $\text{Ly}\alpha$ radiative transfer code MoCALATA (Laursen et al. 2009a), calculated the full radiative transfer equations in simulated galaxies, obtaining an anticorrelation between f_{esc} and galactic size, from order unity to order a few per cent.

Similarly, although Hayes et al. (2010) found that an *average* $f_{\text{esc}} = 5.3\%$ adequate to explain their observations, their fig. 3 shows a trend of f_{esc} decreasing with $E(B - V)$. Comparing the inferred SFR from [OII] with that of $\text{Ly}\alpha$, an upper limit of $\sim 1\%$ is inferred for the galaxy counterpart of the DLA studied here. The extinction is found to be $A_V \simeq 0.2$ (see below), corresponding to a colour excess of $E(B - V) \simeq 0.06$. The extinction in the

centre of the galaxy is likely to be higher. Furthermore, in calculating $E(B - V)$ Hayes et al. (2010) assume a metallicity of 1/3 solar, whereas the present galactic system was shown to have at least solar metallicity, thus probably resulting in higher extinction. Another possible cause could be that SFRs inferred from [OII] are after all associated with rather large uncertainties, as the mean [OII]/ $\text{H}\alpha$ ratios vary substantially from galaxy to galaxy, up to an order of magnitude (Gallagher et al. 1989; Kennicutt 1992).

4.3 Dust reddening

In Fig. 5, we show the X-shooter spectrum of Q 0918+1636. With a dashed line we show the composite QSO spectrum from Telfer et al. (2002) and it is evident that Q 0918+1636 is redder than the composite spectrum. The evidence for dust in the system comes from the observed strong depletion of refractory elements. In addition, the spectrum of Q 0918+1636 appears substantially redder than the spectra of typical QSOs around $z = 3$. Q 0918+1636 was selected as a candidate high- z QSO based on its red $u^* - g^*$ colour. It falls outside the selection criteria for candidate $z < 3.6$ QSOs in SDSS (Richards et al. 2003). In Fig. 6, we compare the colours of Q 0918+1636 with the colours of QSOs with redshift within 3.07 ± 0.05 from the SDSS DR7 QSO catalogue after removing BAL QSOs (Schneider et al. 2007). As seen, the distributions of QSO colours are relatively narrow. However, the distributions have small extensions towards redder colours and Q 0918+1636 is among the reddest 4%, 0.7% and 12% of QSOs at these redshifts for $u^* - g^*$, $g^* - r^*$ and $r^* - i^*$, respectively. With contours we show the colours of the stellar locus from stripe 82 in the same colours (Ivezić et al. 2007). Only in the $u^* - g^*$ colour has the reddening moved Q 0918+1636 further away from the stellar locus and in these bands the QSO is very faint. Hence, it is very difficult to select reddened QSOs at these redshifts using optical colours. In a future study, we will address how one can select even redder QSOs using photometry in the near-IR bands. The most likely cause of the red colour of Q 0918+1636 is dust in the $z_{\text{abs}} = 2.5832$ DLA given its high metallicity and strong evidence for depletion of refractory elements on dust grains. Dust in the $z = 2.412$ DLA could also contribute, but as mentioned in the introduction this DLA not as metal rich as the $z_{\text{abs}} = 2.5832$ DLA. The presence of dust along the line-of-sight is supported by the fact that the SED of Q 0918+1636 can be well fitted with the composite QSO spectrum from Telfer et al. (2002) reddened by SMC/LMC-like extinction at $z_{\text{abs}} = 2.5832$ with a total amount of extinction given by $A_V = 0.2$ mag. Here, we have used the prescription given in Pei (1992) to model the extinction curve. The agreement with the observed spectrum is very good. It is not possible to get a good fit with the MW extinction curve.

The corresponding extinction-to-gas ratio, $A_V/N(\text{H I}) \approx 2.5 \times 10^{-22} \text{ mag cm}^2$, is in between the ratios inferred from LMC and MW sightlines (e.g. Gordon et al. 2003) and substantially higher than what is found on average for DLAs ($A_V/N(\text{H I}) \sim 2.4 \times 10^{-23} \text{ mag cm}^2$ Vladilo et al. 2008). The fact that reddening has moved Q 0918+1636 to the boundary of the colour space where QSOs are selected in SDSS is consistent with previous studies arguing that metal-rich DLAs most likely are systematically missing from current DLA samples from optical QSO surveys (e.g., Pei et al. 1999 and references therein; Noterdaeme et al. 2009a, 2010; Pontzen & Pettini 2009).

In conclusion, our results support the suggestion of F10 that high-metallicity DLAs are associated with bright galaxy counterparts. The $z_{\text{abs}} = 2.5832$ DLA has a high metallicity (for its red-

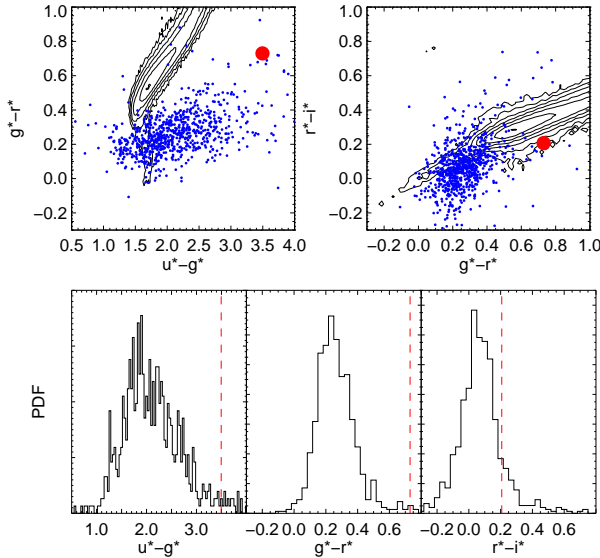


Figure 6. Here, we compare the colours of Q0918+1636 with the colours of other SDSS QSOs within $\Delta z = 0.05$ of the redshift of Q0918+1636 (BAL QSOs excluded). The top two panels show colour-colour diagrams and the lower three panels show the histograms of colours. The contours in the upper panels show the colour distribution of the stellar locus. Q0918+1636 (marked as a circle in the colour-colour plots and a dashed line in the histograms) is among the reddest of all SDSS QSOs in this redshift range (4% in u^*-g^* , 0.7% in g^*-r^* and 12% in r^*-i^*).

shift) of close to solar despite probing a region about 16 kpc away from the central emitting region of the DLA galaxy counterpart. We establish the presence of H_2 absorption, and also dust grains based on the depletion of refractory elements and from reddening of the background QSO.

ACKNOWLEDGMENTS

The Dark Cosmology Centre is funded by the DNRF. We thank our anonymous referee for a fast and constructive report and K. Schmidt and C. Péroux for useful discussions. PN is supported by a CONICYT/CNRS fellowship. PL acknowledges funding from the Villum Foundation. JRM is a Sophie & Tycho Brahe fellow. ST is supported by the Lundbeck foundation.

REFERENCES

Asplund, M., Grevesse, N., Sauval, A. J., & Scott, P., 2009, *ARA&A*, 47, 481
 Cassata, P., Le Fèvre, O., Garilli, B., et al., 2011, *A&A*, 525, A143+
 Charlot, S. & Fall, S. M., 1991, *ApJ*, 378, 471
 Colbert, J. W. & Malkan, M. A., 2002, *ApJ*, 566, 51
 Dayal, P., Ferrara, A., Saro, A., Salvaterra, R., Borgani, S., & Tornatore, L., 2009, *MNRAS*, 400, 2000
 Dutton, A. A., van den Bosch, F. C., & Dekel, A., 2010, *MNRAS*, 405, 1690
 Erb, D. K., Shapley, A. E., Pettini, M., Steidel, C. C., Reddy, N. A., & Adelberger, K. L., 2006, *ApJ*, 644, 813

Fynbo, J. P. U., Laursen, P., Ledoux, C., et al., 2010, *MNRAS*, 408, 2128 (F10)
 Fynbo, J. P. U., Ledoux, C., Möller, P., Thomsen, B., & Burud, I., 2003, *A&A*, 407, 147
 Fynbo, J. P. U., Prochaska, J. X., Sommer-Larsen, J., Dessauges-Zavadsky, M., & Möller, P., 2008, *ApJ*, 683, 321
 Fynbo, J. U., Möller, P., & Warren, S. J., 1999, *MNRAS*, 305, 849
 Gallagher, J. S., Hunter, D. A., & Bushouse, H., 1989, *AJ*, 97, 700
 Gawiser, E., van Dokkum, P. G., Herrera, D., et al., 2006, *ApJS*, 162, 1
 Goldoni, P., Royer, F., François, P., Horrobin, M., Blanc, G., Vernet, J., Modigliani, A., & Larsen, J., 2006, in Presented at the Society of Photo-Optical Instrumentation Engineers (SPIE) Conference, Vol. 6269, Society of Photo-Optical Instrumentation Engineers (SPIE) Conference Series
 Gordon, K. D., Clayton, G. C., Misselt, K. A., Landolt, A. U., & Wolff, M. J., 2003, *ApJ*, 594, 279
 Gronwall, C., Ciardullo, R., Hickey, T., et al., 2007, *ApJ*, 667, 79
 Grove, L. F., Fynbo, J. P. U., Ledoux, C., Limousin, M., Möller, P., Nilsson, K. K., & Thomsen, B., 2009, *A&A*, 497, 689
 Hayes, M., Östlin, G., Schaerer, D., et al., 2010, *Nature*, 464, 562
 Ivezić, Ž., Smith, J. A., Miknaitis, G., et al., 2007, *AJ*, 134, 973
 Kaplan, K. F., Prochaska, J. X., Herbert-Fort, S., Ellison, S. L., & Dessauges-Zavadsky, M., 2010, *PASP*, 122, 619
 Kelson, D. D., 2003, *PASP*, 115, 688
 Kennicutt, Jr., R. C., 1992, *ApJ*, 388, 310
 —, 1998, *ARA&A*, 36, 189
 Kewley, L. J. & Ellison, S. L., 2008, *ApJ*, 681, 1183
 Kulkarni, V. P., Woodgate, B. E., York, D. G., Thatte, D. G., Meiring, J., Palunas, P., & Wassell, E., 2006, *ApJ*, 636, 30
 Lamareille, F., Brinchmann, J., Contini, T., et al., 2009, *A&A*, 495, 53
 Laursen, P., Razoumov, A. O., & Sommer-Larsen, J., 2009a, *ApJ*, 696, 853
 Laursen, P., Sommer-Larsen, J., & Andersen, A. C., 2009b, *ApJ*, 704, 1640
 Laursen, P., Sommer-Larsen, J., & Razoumov, A. O., 2010, *ArXiv e-prints*
 Le Delliou, M., Lacey, C., Baugh, C. M., Guiderdoni, B., Bacon, R., Courtois, H., Sousbie, T., & Morris, S. L., 2005, *MNRAS*, 357, L11
 Le Delliou, M., Lacey, C. G., Baugh, C. M., & Morris, S. L., 2006, *MNRAS*, 365, 712
 Ledoux, C., Bergeron, J., & Petitjean, P., 2002, *A&A*, 385, 802
 Ledoux, C., Petitjean, P., Fynbo, J. P. U., Möller, P., & Srianand, R., 2006, *A&A*, 457, 71
 Ledoux, C., Petitjean, P., & Srianand, R., 2003, *MNRAS*, 346, 209
 Ledoux, C., Srianand, R., & Petitjean, P., 2002b, *A&A*, 392, 781
 Maiolino, R., Nagao, T., Grazian, A., et al., 2008, *A&A*, 488, 463
 Mannucci, F., Cresci, G., Maiolino, R., Marconi, A., & Gnerucci, A., 2010, *MNRAS*, 408, 2115
 Meyer, D. M. & Roth, K. C., 1990, *ApJ*, 363, 57
 Möller, P. & Warren, S. J., 1998, *MNRAS*, 299, 661
 Möller, P., Fynbo, J. P. U., & Fall, S. M., 2004, *A&A*, 422, L33
 Möller, P. & Warren, S. J., 1993, *A&A*, 270, 43
 Möller, P., Warren, S. J., Fall, S. M., Fynbo, J. U., & Jakobsen, P., 2002, *ApJ*, 574, 51
 Noterdaeme, P., Ledoux, C., Petitjean, P., & Srianand, R., 2008, *A&A*, 481, 327
 Noterdaeme, P., Ledoux, C., Srianand, R., Petitjean, P., & Lopez, S., 2009a, *A&A*, 503, 765

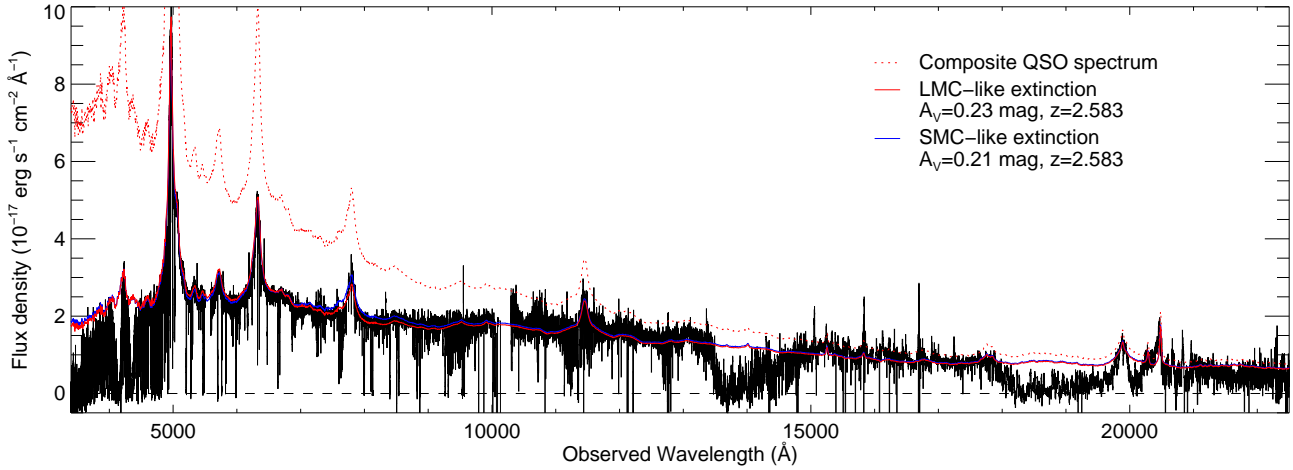


Figure 5. The spectrum of Q0918+1636 after flux calibration. The overall shape of the spectrum is well fitted by the composite QSO spectrum from Telfer et al. (2002). In the figure, the unreddened composite spectrum is shown with a dashed line, and the same spectrum reddened by SMC- and LMC-like extinction curves with rest frame $A_V = 0.2$ mag is shown with solid red and blue lines, respectively. The inferred dust-to-gas ratio is between those of the LMC and the MW. The spectrum has been corrected for galactic extinction with $E(B - V) = 0.025$ from Schlegel et al. (1998).

Noterdaeme, P., Petitjean, P., Ledoux, C., López, S., Srianand, R., & Vergani, S. D., 2010, *A&A*, 523, A80+
 Noterdaeme, P., Petitjean, P., Ledoux, C., & Srianand, R., 2009b, *A&A*, 505, 1087
 Noterdaeme, P., Petitjean, P., Srianand, R., Ledoux, C., & Le Petit, F., 2007, *A&A*, 469, 425
 Ouchi, M., Shimasaku, K., Akiyama, M., et al., 2008, *ApJS*, 176, 301
 Pei, Y. C., 1992, *ApJ*, 395, 130
 Pei, Y. C., Fall, S. M., & Hauser, M. G., 1999, *ApJ*, 522, 604
 Petitjean, P., Ledoux, C., Noterdaeme, P., & Srianand, R., 2006, *A&A*, 456, L9
 Pettini, M., King, D. L., Smith, L. J., & Hunstead, R. W., 1997, *ApJ*, 478, 536
 Pontzen, A. & Pettini, M., 2009, *MNRAS*, 393, 557
 Prochaska, J. X., Herbert-Fort, S., & Wolfe, A. M., 2005, *ApJ*, 635, 123
 Rahmani, H., Srianand, R., Noterdaeme, P., & Petitjean, P., 2010, *MNRAS*, 409, L59
 Rauch, M., Haehnelt, M., Bunker, A., et al., 2008, *ApJ*, 681, 856
 Rauch, M. & Haehnelt, M. G., 2010, *ArXiv e-prints*
 Reddy, N. A. & Steidel, C. C., 2009, *ApJ*, 692, 778
 Richards, G. T., Hall, P. B., Vanden Berk, D. E., et al., 2003, *AJ*, 126, 1131
 Savaglio, S., Glazebrook, K., Le Borgne, D., et al., 2005, *ApJ*, 635, 260
 Sawicki, M. & Thompson, D., 2006, *ApJ*, 642, 653
 Schlegel, D. J., Finkbeiner, D. P., & Davis, M., 1998, *ApJ*, 500, 525
 Schneider, D. P., Hall, P. B., Richards, G. T., et al., 2007, *AJ*, 134, 102
 Smith, H. E., Cohen, R. D., Burns, J. E., Moore, D. J., & Uchida, B. A., 1989, *ApJ*, 347, 87
 Srianand, R., Petitjean, P., Ledoux, C., Ferland, G., & Shaw, G., 2005, *MNRAS*, 362, 549
 Telfer, R. C., Zheng, W., Kriss, G. A., & Davidsen, A. F., 2002, *ApJ*, 565, 773
 Tremonti, C. A., Heckman, T. M., Kauffmann, G., et al., 2004, *ApJ*, 613, 898

van Dokkum, P. G., 2001, *PASP*, 113, 1420
 Vladilo, G., Prochaska, J. X., & Wolfe, A. M., 2008, *A&A*, 478, 701
 Wolfe, A. M., Gawiser, E., & Prochaska, J. X., 2005, *ARA&A*, 43, 861
 Wolfe, A. M., Prochaska, J. X., Jorgenson, R. A., & Rafelski, M., 2008, *ApJ*, 681, 881